Vesicle-vesicle adhesion by mobile lock-and-key molecules: Debye-Hückel theory and Monte Carlo simulation

Daniel M. Zuckerman
Institute for Physical Science and Technology, University of Maryland, College Park, Maryland 20742

Robijn F. Bruinsma
Department of Physics, University of California at Los Angeles, Los Angeles, California 90095

(Received 11 December 1996)

Adhesion between cells is due to formation of weak, reversible chemical bonds between ''lock'' and ''key'' molecules imbedded in the cell surfaces. In this paper we present a theory for cell adhesion that extends the well-known Bell model of noninteracting adhesion molecules to include the cell-surface mediated elastic coupling between the molecules. We show that the statistical mechanics of this many-body problem can be mapped onto that of the two-dimensional Coulomb plasma with attractive forces. Using this mapping we find the following results: (i) the ideal-mixing state assumed by Bell and co-workers [Science **200**, 618 (1978); Biophys. J. **45**, 1051 (1984)] is unstable against migration of adhesion molecules to the rim of the adhesion disk in agreement with experimental observations and (ii) loss of adhesion is generally preceded by the collapse of the adhesion disk into a ''stress-focused'' state with enhanced adhesive strength.
[S1063-651X(98)08901-6]

PACS number(s): 87.22.Nf, 87.15.Kg

I. INTRODUCTION

Cell-cell recognition and adhesion through cellular adhesion molecules is a fundamental process in biology, central to embryological development, tissue stability, and immunology. Great progress has been made in the isolation, structure determination, and biochemistry of adhesive proteins and of molecular recognition by proteins in general. In the immune system, for example, the molecular basis of antibody-antigen recognition is the interaction between the membrane-bound immunoglobin (Ig) molecules of leukocytes (and lymphocytes) with foreign molecules, such as lipopolysaccharides attached to bacterial membranes [1]. The molecular basis for cell-cell recognition during embryological development [2] is the homophilic binding of membrane-bound cellular adhesion molecules (CAMs) such as *N*-CAMs, *P*-CAMs, and cadherins.

The physical characterization of bioadhesion is attracting increasing interest, but there remain significant obstacles. The difficulties stem from the fact that, on the one hand, the interaction between a particular pair of ''lock-and-key'' molecules is far from simple, depending as it does on the details of the molecular architecture, while, on the other hand, adhesion molecules are embedded in a cell membrane and frequently attached to the cytoskeleton (which can transmit signals from the adhesion molecules [3]). Certain important features are nonetheless becoming clear. Force measurements between adhesion molecules by atomic force microscopy [4], the force box [5], and other experiments [6] indicate that forces of order 50–200 pN are required to break the chemical bonds between typical adhesion molecules. This fracture force, however, is sensitively dependent on the rate at which the force is applied [7]. Equilibrium binding energies (E_B) measured from chemical equilibrium constants are of order $5k_BT$ for selectins and their sugar ligands [8], but considerably higher for integrins. For Ig molecules, they are in the range $10k_BT-20k_BT$ [1]. This is a sensible range for ''signaling'' molecules, from a design perspective, since molecular bonds of strength less than k_BT would not withstand thermal fluctuations, while chemical bonds with an energy much greater than k_BT would be too ''costly'' to remove [9]. Typical cell-cell adhesion involves of order 10^3-10^4 adhesion molecules, so the total adhesion energy between two cells is substantial. Cell adhesion thus should be described *statistically*: The cooperative effect of many weak molecular bonds collectively creates a strong adhesion.

A major part of our physical understanding of cell-cell adhesion comes from a model developed by Bell and coworkers [10]. The Bell model describes cell adhesion as the competition between two opposing mechanisms. First, there is a generic repulsion between the cells due to the osmotic pressure of the membrane lipo-polysachharides (the glycocalix) that are squeezed between the cell surfaces. The range of this repulsion is about 500–1000 Å. This repulsion then competes with the above-mentioned specific bonding between lock-and-key molecules. Pure phospholipid bilayers containing neither lock-and-key molecules nor lipopolysachharides interact through a combination of van der Waals attraction and double-layer electrostatic repulsion. This leads to an adhesion energy of order $k_BT/(50\ \text{Å}^2)$ [11]. This nonspecific adhesion, which is undesirable, is prevented by the glycocalix repulsion, while the lock-and-key molecules allows for a more refined regulation of the adhesion process.

Bell and co-workers [10] treated the lock-and-key molecules as an ideal (i.e., noninteracting) two-dimensional reactive solution where reactants L (for lock) and K (for key) are in chemical equilibrium with the reaction produced LK so $L+K \rightleftharpoons LK$. This assumption allowed them to compute an adhesion free energy G. Once the adhesion free energy is known one can determine whether or not cells adhere as well as the shape of adhering cells using the continuum elastic theory of cell membranes [12]. Continuum theory relates the

contact angle of a cell adhering to a substrate to the adhesion free energy and the tension of the cell wall through Young's law, borrowed from the theory of wetting [13]. The results appear to be confirmed by micropipette studies of cell adhesion [14]. In addition, continuum theory also predicts the suppression of thermal shape fluctuations [15] in strongly adhering cells, which has been confirmed experimentally [16]. From the viewpoint of a physical description, the Bell model is quite attractive. As discussed in more detail in Sec. III, it allows us to include the biochemical complexity of protein-protein recognition through a small number of measurable quantities from which we can deduce the effective adhesion strength. It also can be extended to include dynamic processes [17].

There are nevertheless experimental observations that appear to be in disagreement with the model. Studies of the adhesion of *T* cells to target cells by Tozeren, Sung, and Chien [18] revealed that the adhesion disk connecting the cells is *inhomogeneous* with adhesion molecules migrating to the rim of the disk. Similar phenomena were also reported by Chen, Helm, and Israelachevilli [19]. Numerical simulations of plate adhesion by polymers [20] show, in detail, that when the plates are pulled apart, the adhesive layer decomposes into stress-focused regions with higher concentration of adhesion molecules and cavities with low concentrations. Eventually, only a few bridges are left and cavities form everywhere.

It is the basic premise of this paper that the Bell model is sound but that the ideal-solution approximation is invalid. The assumption of weak interaction between adhesion molecules seems to be quite reasonable at first sight. The mean spacing between the 10^3-10^4 adhesion molecules in a 1-μm adhesion disk is about 100 Å, long enough to exclude direct interactions as a significant effect. Braun and co-workers [21] nevertheless suggested that adhesion molecules do interact, but *indirectly*. They proposed that cell-cell repulsion by the glycocalix generates a long-range attraction between adhesion molecules, *mediated by the cell membranes*. Theoretical analysis of the stresses in adhering membranes [22] confirmed this concept and predicted an attractive potential between adhesion molecules that increases with spacing r as $\ln r$. In this paper we generalize the Bell model to include the indirect interaction between adhesion molecules. The statistical properties of this many-body system are studied by a combination of statistical-mechanics methods and Monte Carlo simulation. Some of the mathematical features of this model were presented earlier in a brief report [23].

We define our model in Sec. II, where we also review the continuum theory of adhesion. In Sec. III we restrict ourselves to noninteracting adhesion molecules. In that limit we reproduce the ideal-solution theory of Bell and co-workers [10]. In Sec. IV we include the correlations between the adhesion molecules and show that this leads to a many-body problem equivalent to a two-dimensional (2D) plasma of ''charges'' interacting with an attractive logarithmic potential in a neutralizing background. We discuss the general structure of the free energy and demonstrate that it has a singularity as we increase the coupling constant. We then borrow a method from plasma physics, specifically Debye-Hückel theory, to show that the state of uniform mixing of adhesion molecules implicit in the Bell model is *unstable for arbitrarily small values of the coupling constant*. This is only true in the thermodynamic limit of many adhesion molecules. For a finite number of adhesion molecules, there is a small range where the uniform state is stable. In Sec. V we show the result of a Monte Carlo simulation. We find that the distribution of adhesion molecules is indeed inhomogeneous with the adhesion molecules collecting at the rim of the adhesion disk. As we increase the coupling constant, we find that the adhesion molecules collapse into a single patch when the dimensionless coupling constant exceeds a value of order one, which may be the singularity in the free energy found in Sec. IV. Finally, in Sec. VI we construct the adhesion phase diagram shown in Fig. 1, our main result. The horizontal axis γ in Fig. 1 is the tension of the cell surface and the vertical axis is the glycocalix disjoined pressure p. The horizontal dotted line is the critical pressure $p_T^{(0)}$ for cell separation found from the Bell model with no interaction.

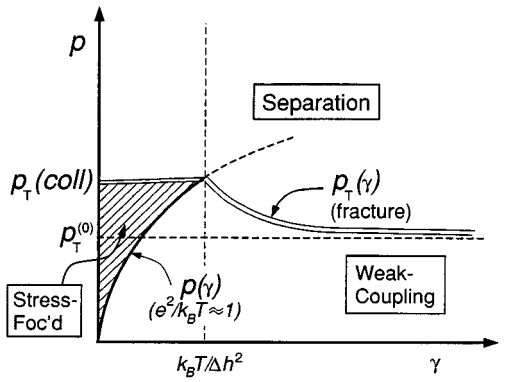

FIG. 1. Phase diagram with p the glycocalix pressure and γ the tension. The heavy line indicates the collapse of the disk. The double line is the threshold for loss of adhesion $p_T(\gamma)$. The horizontal dashed line is the threshold pressure of the Bell model.

The part of the phase diagram labeled ''weak coupling'' corresponds to an inhomogeneous adhesion disk with adhesion molecules mostly distributed around the rim. Increasing p leads to fracture of adhesion at the double line labeled $p_T(\gamma)$. For large γ, $p_T(\gamma)$ approaches the fracture pressure $p_T^{(0)}$ of the noninteracting Bell model. As we reduce γ, we reach the boundary marked $p(\gamma)$, where the adhesion molecules collapse into a single cluster. The adhesive strength of the single cluster, $p_T(\text{coll})$, exceeds the ideal solution value $p_T^{(0)}$ by a considerable amount provided the lock-and-key binding energy E_B exceeds k_BT significantly. We conclude with a discussion of the relevance of our results.

II. ADHESION HAMILTONIAN

We construct in this section an effective Hamiltonian to describe the adhesion between two cells with mobile ''lock'' (L) molecules embedded in one cell and mobile ''key'' (K) molecules in the other cell [24]. The cells are treated in a simplified way: as two vesicles (i.e., closed surfactant bilayers) with embedded adhesion molecules. Our model is pictured in Fig. 2. In Fig. 2(a) we show two simplified cells adhering by lock-and-key (LK) molecules at a small circular contact patch, which is shown in enlarged cross section in Fig. 2(b). In the enlargement, we see bound lock-and-key pairs separated by areas where the membranes ''billow'' out

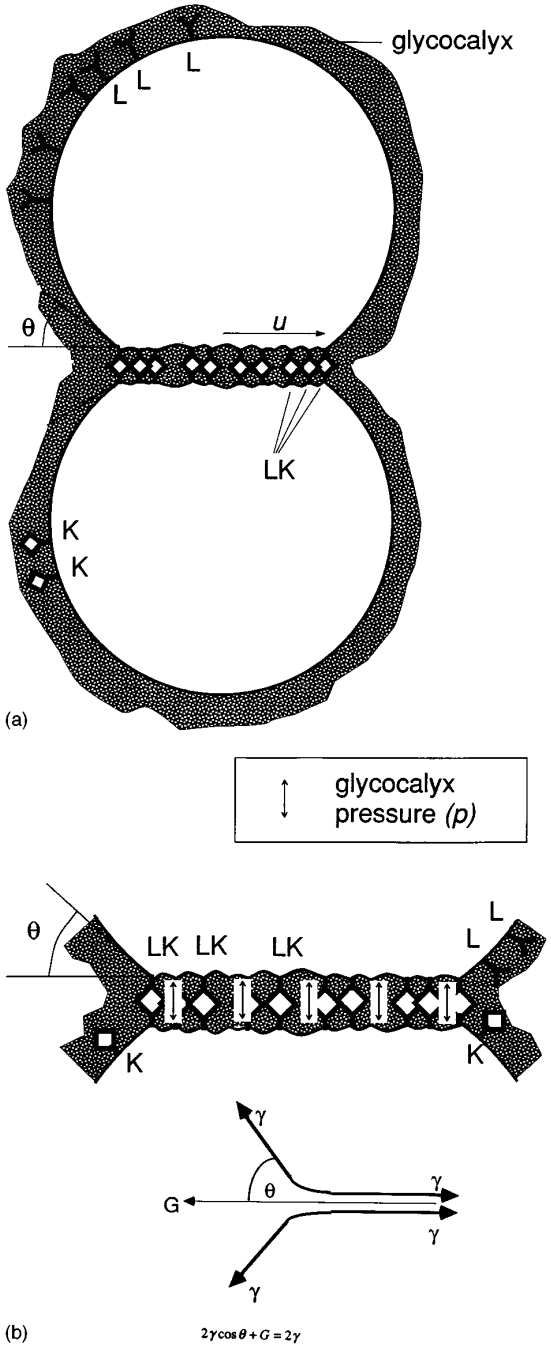

FIG. 2. (a) Two model cells adhering by lock-and-key adhesion. The upper vesicle only carries locks (L), the lower only keys (K). The adhesion complexes are denoted LK. The radius of the adhesion disk is u, the vesicle radius is R', and the contact angle between the two vesicles is θ. The hatched coat on each cell is the glycocalix (lipo-polysachharides embedded in the membranes). (b) The repulsive pressure of the glycocalyx produces billowing out of the membrane in between LK sites. This in turn leads to attraction and stress focusing. The contact angle θ is determined by Young's law as shown.

due to repulsive pressure from the glycocalyx. We assume that lock-and-key pairs force only a modest local compression of the glycocalyx.

We now write the adhesion Hamiltonian as a sum of three parts

$$H = H_{\rm el} + H_{\rm glyc} + H_{\rm LK}. \tag{1}$$

The first term $H_{\rm el}$ is the continuum elastic energy of the vesicle, $H_{\rm glyc}$ is the glycocalyx contribution, and $H_{\rm LK}$ is the Hamiltonian of the lock-and-key adhesion molecules. We will discuss the three terms separately in the following subsections.

A. Elastic energy: Continuum theory

The elastic energy of a (symmetric) bilayer vesicle is, in the simplest continuum theory [25], given by

$$H_{\rm el} = \frac{1}{2}\,\kappa \int\int_{\rm surface} \left(\frac{1}{R_1} + \frac{1}{R_2}\right)^2 + \gamma A - \Pi V. \tag{2}$$

In the first term, κ is the Helfrich bending energy (typically of order $10k_BT - 100k_BT$) and R_1, R_2 are the principal radii of curvature. In the second term, γ is the tension of the vesicle and A its surface area. For the third term, Π is the osmotic pressure difference between the vesicle's interior and exterior and V denotes the volume. For a nonadhering vesicle, $H_{\rm el}$ is minimized by $R_1 = R_2 = R$, i.e., a sphere, with $\Pi = 2\gamma/R$ (Laplace's law).

Upon adhering together, the vesicles may deform, in which case they take the (approximate) shape of *truncated spheres* as shown in Fig. 2(a). The new vesicle radius will be called R' and the area of contact πu^2, with u the radius of the contact disk. Cells maintain their volume, so we will assume that the volume V is fixed during the process of adhesion. However, because of the possibility of the smoothing of the ruffles in the cell surface, generated by the tension of the cytoskeleton, the effective surface area of a cell is not fixed. We can quantify this by noting that it follows from geometrical considerations that

$$R' - R \approx \frac{u^4}{16R^3}. \tag{3}$$

for $u/R \ll 1$, while the area A increases by an amount

$$\Delta A \approx \frac{\pi u^4}{4R^2}. \tag{4}$$

Using Eqs. (3) and (4), one finds that the elastic energy increases by an amount

$$\Delta H_{\rm el} \approx \frac{\pi}{2}\,\gamma\,\frac{u^4}{R^2} - \pi\kappa\,\frac{u^2}{R^2} + 2\pi u\tau, \tag{5}$$

assuming $u/R \ll 1$. The first term represents the work done by the tension γ as the vesicle surface area increases by ΔA. The second term is the reduction in bending energy due to flattening the contact disk. The final term gives the energy cost of the high degree of bending that occurs at the rim of the adhesion disk. It has the form of a line energy with line tension τ. A functional minimization of Eq. (2) shows [12] that, within continuum theory,

$$\tau \simeq \frac{3}{4}\,\sqrt{\frac{\kappa}{\gamma}}\,G, \tag{6}$$

with G the adhesive energy per unit area of the contact disk.

As a simple illustration of Eq. (5), we add an adhesive energy $-G\pi u^2$ to $\Delta H_{\rm el}$ and obtain the following mean-field, continuum expression for the free energy:

$$\Delta F_{\rm cont}(u) = -G\pi u^2 + \frac{\pi}{2}\,\gamma\,\frac{u^4}{R^2} + 2\pi u\tau, \tag{7}$$

where we assume $\kappa/R^2 \ll G$, which is the case under all practical conditions. We plot $\Delta F_{\rm cont}(u)$ for typical parameters in Fig. 3. There are, in general, two local minima of $\Delta F(u)$: one at $u=0$ and one at finite u. A first-order phase transition occurs near $G=0$ when the global minimum shifts from $u=0$ to finite u. We will refer to the $u=0$ minimum as ''microadhesion,'' which itself describes two possible scenarios: either (i) only a small number of adhesion molecules are involved in the binding with the two adhering vesicles that are essentially spherical or (ii) there is no adhesion at all. A minimum of $\Delta F_{\rm cont}(u)$ at finite u represents ''collective adhesion'' involving many adhesion molecules. The collective adhesion minimum of $\Delta F(u)$ obeys, for small G/γ,

$$u^* \simeq R\left(\frac{G}{\gamma}\right)^{1/2}. \tag{8}$$

An alternative way to arrive at Eq. (8) is shown in Fig. 2. In equilibrium, the force per unit length on the rim of the adhesion disk must vanish. This is the case if $G + 2\gamma\cos\theta = 2\gamma$, with θ the *contact angle* between the cells, measured from the contact plane. This is just Young's law for three-phase contact lines [13]. Figure 2(a) shows that $\theta \simeq (G/\gamma)^{1/2}$ for small θ, together with $\theta \cong u/R$ leading to Eq. (8). The collective adhesion minimum of the free energy thus corresponds to Young's law.

The point where the two minima are degenerate can be expressed in terms of the vesicle size R. Collective adhesion should occur when the vesicle radius exceeds a critical value given approximately by

$$R_c \simeq \left(\frac{\kappa}{G}\right)^{1/2}. \tag{9}$$

Vesicles with radii $R < R_c$ will be spherical (and at best microadherent), while those with $R > R_c$ will have a finite adhesion disk that obeys Eq. (8). One of the aims of this paper is to find out whether this simple ''mean-field'' picture remains valid if we allow for the internal degrees of freedom of adhesion.

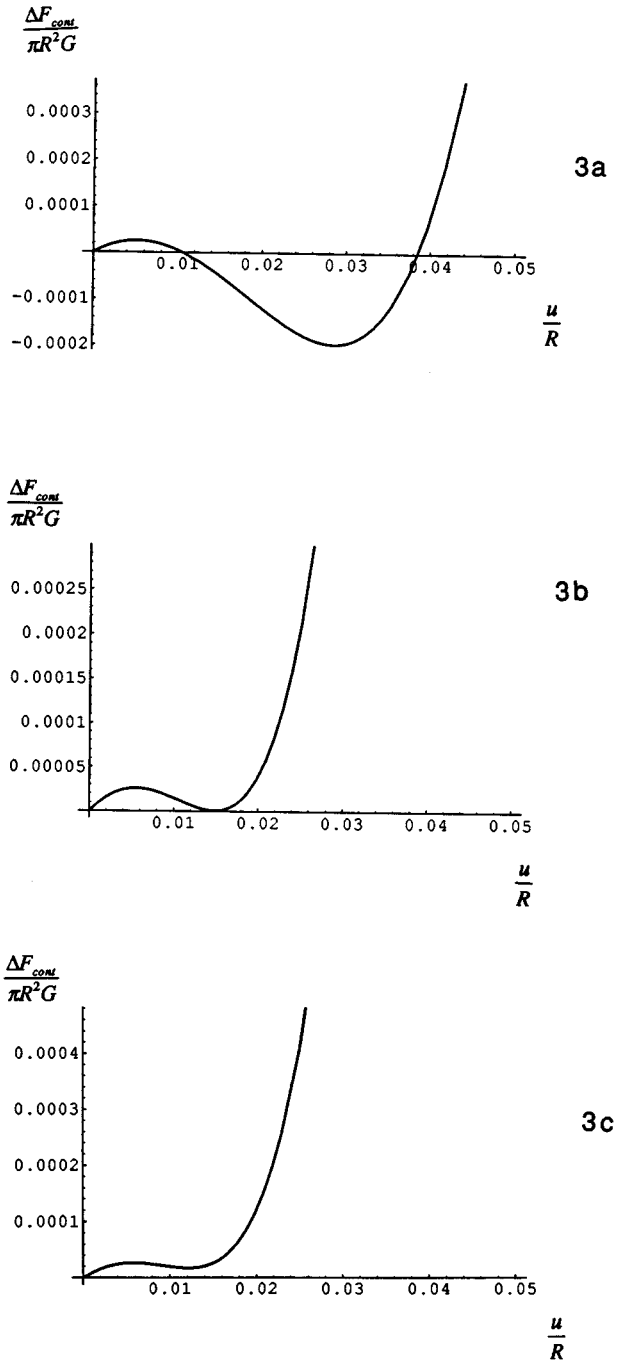

FIG. 3. Continuum theory of adhesion energy $\Delta F_{\rm cont}(u)$ as a function of the radius u of the adhesion disk. (a) shows a finite u global minimum. (b) As G, the adhesion energy, decreases the global minimum shifts to $u=0$ at a critical point. The parameter values are as follows. The dimensionless adhesion energy $2G/\gamma$ equals (a) 2×10^{-3}, (b) 6.7×10^{-4}, and (c) 5×10^{-4}. The dimensionless line tension $2\tau/RG = 0.01$ for all three cases.

B. Lock-and-key adhesion

Our next step is to construct the Hamiltonian for the lock and key molecules [$H_{\rm LK}$ of Eq. (1)]. Following Bell and co-workers [10], we assume that the molecular bonds are fully reversible and that the bound adhesion complexes, like the unbound adhesion molecules, are mobile within the two-dimensional contact area. We assume that each adhering vesicle possesses N adhesion molecules in total, with one vesicle containing only L molecules and one only K molecules. The L and K molecules can bond, forming LK complexes, of quantity M and chemical binding energy E_B. Hence we have M freely mobile LK molecules in the contact region, while $N-M$ unbound adhesion molecules roam each vesicle. We further assume the LK molecules to have an infinitely repulsive hard core of radius a_0. The lock-and-key Hamiltonian will contain three parts: (i) the binding energy $(-ME_B)$ for the LK complexes, (ii) the hard-core repulsions, and (iii) the energy cost of deforming the membranes while maintaining the proper LK ''pinning'' separations. This last term is due to the fact that the lock-and-key com-

plexes pin the two membranes together [see Fig. 2(b)], causing compression dimples in the glycocalyx at these pinning sites. Given the tension in the membranes, then, one can visualize the contact region as a dimpled seat cushion, with mobile dimples.

We let $h(\vec{r})$ represent the spacing between the two membranes in the contact disk and let the set $\{\vec{R}_i\}$, with $i=1,\ldots,M$ denote the locations of the LK complexes within the adhesion disk. The pinning constraints are thus

$$h(\vec{R}_i)=h_{\mathrm{LK}}, \quad i=1,\ldots,M, \tag{10}$$

with h_{LK} the fixed spacing at the LK sites. We account for the elastic energy cost of the dimples by adding to the Hamiltonian

$$\tfrac{1}{2}\gamma\int d^2r(\vec{\nabla}h)^2, \tag{11}$$

where the integral multiplying the tension γ is the excess area of the dimples.

We must also include a term that prevents the complexes, of finite molecular diameter a_0, from overlapping. This will consist of standard hard-core potentials

$$V(|\vec{R}_i-\vec{R}_j|)=\begin{cases}\infty & \text{for } |\vec{R}_i-\vec{R}_j|<a_0\\ 0 & \text{for } |\vec{R}_i-\vec{R}_j|\geqslant a_0.\end{cases} \tag{12}$$

Putting all the terms together, we can explicitly write the LK Hamiltonian as

$$H_{\mathrm{LK}}[h]=-ME_B+\sum_{i<j}V(|\vec{R}_i-\vec{R}_j|)+\tfrac{1}{2}\gamma\int d^2r(\vec{\nabla}h)^2, \tag{13}$$

where the integral is to be performed over the contact disk only.

C. Glycocalyx

The final contribution to the lock-and-key Hamiltonian is the compression energy of the glycocalyx. The glycocalyx is essentially a ''brush'' of charged macromolecules (oligosachharides) extending out of the membranes. The portions of the membranes in the contact disk are repelled from one another due to osmotic pressure produced by confinement of the charged macromolecules and their counterions inside the adhesion disk. The thickness h_{glyc} is typically of order 100–300 Å.

The osmotic pressure of a compressed polyelectrolyte brush is primarily due to the counterions and obeys 't Hooft's law $\Pi=nk_BT$, where n is the concentration of counterions. For the glycocalyx,

$$\Pi=\frac{z\varphi}{h}k_BT, \tag{14}$$

with φ the area density of charged macromolecules, z the number of charges per macromolecule, and h the intermembrane spacing, assumed here to be only slightly less than the glycocalyx thickness h_{glyc}. For a modestly compressed glycocalyx, it is then easy to show that

$$H_{\mathrm{glyc}}\simeq p_{\mathrm{glyc}}\int d^2r[h_{\mathrm{glyc}}-h(\vec{r})], \tag{15}$$

with $p_{\mathrm{glyc}}\simeq zk_BT\varphi/h_{\mathrm{glyc}}$. This would seem to be a naive approximation: h_{glyc} really is only the *mean* height of the oligosachharides, whereas the concentration profile of a polyelectrolyte brush is a smoothly varying function of the distance from the anchored ends. To see why the approximation is valid, first note that we shall be concerned with the biologically relevant case $h_{\mathrm{LK}}\simeq h_{\mathrm{glyc}}$, i.e., the L and K molecules are comparable in size to the oligosachharides. Now let $V(h)$ be the full intermembrane repulsive energy per unit area generated by the glycocalyx, with h the membrane-membrane spacing. The function $V(h)$ surely is monotonically decreasing with h, so $V'(h)<0$. If we are only interested in the range $h\simeq h_{\mathrm{glyc}}\simeq h_{\mathrm{LK}}$, we can always expand

$$V(h)\approx V(h_{\mathrm{glyc}})+(h-h_{\mathrm{glyc}})V'(h_{\mathrm{glyc}})+\cdots, \tag{16}$$

with $V'(h_{\mathrm{glyc}})<0$. Integrating over the adhesion disk again gives Eq. (15) if we identify $p_{\mathrm{glyc}}=-V'(h_{\mathrm{glyc}})$. Note that p_{glyc} has the dimensions of pressure. It is the repulsive force per unit area exerted on the cell surface and we will refer to it as the disjoining pressure. Equation (15) is thus generally applicable when the LK link produces only a mild local deformation of the glycocalyx. If the LK links are significantly shorter than h_{glyc}, then nonlinear terms would have to be included in Eq. (16).

We finally are in a position to write down the full Hamiltonian

$$H=\frac{1}{2}\gamma\int d^2r(\vec{\nabla}h)^2+\frac{1}{2}\sum_{i\neq j}V(\vec{R}_i-\vec{R}_j)-ME_B + p_{\mathrm{glyc}}\int d^2r[h_{\mathrm{glyc}}-h(\vec{r})]+\frac{\pi}{2}\gamma\frac{u^4}{R^2}+2\pi u\tau. \tag{17}$$

The integrals here are constrained by the pinning condition (10).

III. IDEAL SOLUTION THEORY

We can view the lock-and-key description of adhesion, under conditions of thermal equilibrium, as one of *chemical equilibrium* [10]. A reservoir of reagents L (the first vesicle) is in contact with another reservoir of reagents K (the second vesicle). In the region of contact, the L's and K's can react reversibly,

$$L+K\rightleftharpoons LK, \tag{18}$$

forming a product LK and releasing a binding energy E_B. The area concentrations of reagents $[L]$ and $[K]$ and of reaction products $[LK]$ must then obey the equilibrium theory of ideal chemical solutions

$$\frac{[LK]}{[L][K]}=K_{\mathrm{eq}}(T), \tag{19}$$

where $K_{\mathrm{eq}}(T)\propto\exp(E_B/k_BT)$ is the temperature-dependent equilibrium constant (in chemical literature, E_B is referred to

as the ''standard free-energy change'' of the reaction). This relation assumes that, apart from the chemical reaction [Eq. (18)], the reagents and products do not interact. In the notation of Sec. II, $[LK]=[M]=M/\pi u^2$. If $M \ll N$, then $[L] \simeq [K] \simeq [N]=N/4\pi R^2$. In that case, Eq. (19) reduces to $[M]=[N]^2 K_{\rm eq}$.

The free energy ΔF computed from the adhesion Hamiltonian H of Sec. II must reproduce the ideal solution result, if we drop the LK-LK interactions. We do this by setting $h(\vec{r})=h_{\rm LK}$ everywhere, i.e., by assuming a flat profile for the membrane spacing, thus forbidding any dimples and any elastic coupling. The glycocalix is then compressed by an amount $h_{\rm glyc}-h_{\rm LK}$. This yields an ''ideal-solution'' Hamiltonian

$$H_{\rm IS}=-ME_B+p(h_{\rm glyc}-h_{\rm LK})\pi u^2+2\pi u\tau+\frac{\pi}{2}\gamma\frac{u^4}{R^2}. \tag{20}$$

The ideal-solution free energy ($\Delta F_{\rm IS}$), then, will include the internal energy $E_{\rm IS} \simeq H_{\rm IS}$ along with the appropriate entropic terms for the three ideal solutions (of L's, K's, and LK's)

$$\begin{aligned}\Delta F_{\rm IS}(u,M)=&-ME_B+p(h_{\rm glyc}-h_{\rm LK})\pi u^2+2\pi u\tau\\&+\frac{\pi}{2}\gamma\frac{u^4}{R^2}+k_BT\left\{M\ \ln\left(\frac{M}{\pi u^2}\,a^2\right)-M\right.\\&\left.+2(N-M)\ln\left(\frac{N-M}{4\pi R^2}\,a'^2\right)-2(N-M)\right\}.\end{aligned} \tag{21}$$

Here a^2 and a'^2 are molecular size areas. When computing the adhesion free energy per unit area G, we must always subtract from ΔF the free energy $2Nk_BT\ \ln(Na'^2/e^2 4\pi R^2)$ of separated vesicles. Minimization of $\Delta F_{\rm IS}(u,M)$ with respect to M indeed confirms the ideal-solution result. Explicitly, the equilibrium value $M_{\rm IS}$ for the number of LK molecules is

$$M_{\rm IS} \approx \pi u^2 [N]^2 e^{(E_B/k_BT)}\left(\frac{a'^2}{a}\right)^2, \tag{22}$$

with a'^2/a representative of the molecular-size range of the LK interaction and E_B assumed to be of order k_BT.

By replacing M by $M_{\rm IS}$ in Eq. (21), we can now write the free energy $\Delta F_{\rm IS}$ as a function of the single variable u, which will enable a comparison with our results from the simple continuum model of Sec. II:

$$\Delta F_{\rm IS}(u,M=M_{\rm IS})=-G_{\rm IS}\pi u^2+\frac{\pi}{2}\gamma\frac{u^4}{R^2}+2\pi u\tau, \tag{23}$$

where

$$G_{\rm IS} \simeq k_BT[N]^2\left(\frac{a'^2}{a}\right)^2 e^{(E_B/k_BT)}-p(h_{\rm glyc}-h_{\rm LK}), \tag{24}$$

where we have dropped the subscript in the disjoining pressure $p_{\rm glyc}$, a convention followed for the remainder of the paper. We have written $\Delta F_{\rm IS}$ in the same form as the $\Delta F_{\rm cont}$ deduced earlier from continuum theory [Eq. (7)], except that here we have an explicit form for the adhesion free-energy density G.

The discussion of Sec. II remains valid and we expect again a (weak) first-order separation transition near $G_{\rm IS}=0$ if we decrease the binding energy E_B or increase the disjoining pressure p. Note that the adhesion free energy $G_{\rm IS}$ is very sensitive to E_B because of the exponential factor. Changes in adhesion behavior thus can be regulated efficiently by altering E_B (for example, through changes in the pH level). We will later construct a phase diagram for adhesion in the γ-p plane. For the ideal-solution theory, this phase diagram is very simple: The boundary between adhesion and fracture is set by $G_{\rm IS}=0$. In the γ-p, this corresponds to a critical disjoining pressure

$$p_T^{(0)}=k_BT[N]^2\left(\frac{a'}{a}\right)^2\frac{e^{E_B/k_BT}}{h_{\rm glyc}-h_{\rm LK}}, \tag{25}$$

which is independent of the vesicle tension γ. Correcting for the fact that this is really a weak first-order transition at finite $G_{\rm IS}$ does not materially alter this result. Ideal-solution theory thus agrees with the earlier continuum arguments, but gives more precise information regarding the adhesion internal degrees of freedom.

From the physical viewpoint, Eq. (24) is very attractive. The complexity of thousands of mobile adhesion molecules, each of which has a nontrivial architecture, is replaced by a single number $G_{\rm IS}$, which depends on a limited number of parameters: $[N]$, E_B, a'^2/a, p, and $\Delta h=h_{\rm glyc}-h_{\rm LK}$, which at least in principle can be accessed experimentally. As discussed in Sec. VII, if we put in reasonable values for these parameters for T cell adhesion, one finds values for G in the range 0.1–1 dyn/cm, which agrees well with micropipette studies of T cell adhesion [18]. Nevertheless, we have seen in the Introduction that adhesive bonds under stress develop a heterogeneous structure, which requires a more detailed analysis including correlations between adhesion molecules. We will address this in the next section.

IV. CORRELATION ENERGY

In this section we will derive the indirect interactions occurring among the bound LK complexes. The interactions are due to the interplay between membrane tension and glycocalyx pressure, as first proposed by Braun and co-workers. We will use the free energy computed in this section to construct a phase diagram in Sec. V.

A. Attractive Coulomb plasma

In our model the LK molecules couple to each other in two ways: *directly*, as described by the short-range pair potentials $V(|\vec{R}_i-\vec{R}_j|)$ in Eq. (17), and *indirectly*, mediated by the membrane. Under typical conditions, the adhesion molecules have area concentrations that are low enough for direct interactions to be very weak. In the remainder of this section, therefore, we focus on the long-range, indirect coupling, although we will see later that the direct interaction actually plays a key role.

The indirect coupling is generated by the combined effect of the first and fourth terms in Eq. (17) (i.e., the elastic tension and the disjoined pressure). We denote the sum of these two terms $H_{\rm int}$:

$$H_{\rm int}\equiv\tfrac{1}{2}\gamma\int d^2r(\vec{\nabla}h)^2+p\int d^2r[h_{\rm glyc}-h(\vec{r})]. \quad (26)$$

We can find the mechanical equilibrium spacing profile $h^*(\vec{r})$ by minimizing $H_{\rm int}$ with respect to $h(\vec{r})$ while obeying the M constraints $h(\vec{R}_i)=h_{\rm LK}$. This is done by the method of Lagrange multipliers: We minimize

$$W\equiv H_{\rm int}+\sum_{i=1}^{M}\mu_i h(\vec{R}_i) \quad (27)$$

and determine the μ_i by imposing the M constraints. Setting $\delta W/\delta h=0$ gives

$$\gamma\nabla^2 h^*(\vec{r})=-p+\sum_{i=1}^{M}\mu_i\delta(\vec{r}-\vec{R}_j). \quad (28)$$

The positions $\{\vec{R}_i\}$ of the LK molecules vary with the configuration, which implies that the μ_i and h^* are also configuration dependent.

We assume as a boundary condition on the solution of this differential equation that $h(\vec{r})$ is flat at the edge of the adhesion disk. Integrating Eq. (28) over the disk area and applying Gauss's theorem then gives

$$\frac{p}{[M]}=\frac{1}{M}\sum_{i=1}^{M}\mu_i\equiv\mu. \quad (29)$$

That is, the mean of the M Lagrange multipliers is fixed by the glycocalyx pressure p and the LK concentration $[M]$.

Note now the similarity between Eq. (28) and the Poisson equation for a set of like charges in a neutralizing background. We can identify h as the potential of a plasma of M positive charges (of magnitude μ/γ) in a uniform, neutralizing background of negative charge. Equation (29), then, effectively imposes the overall charge neutrality. There is, however, an important difference between the present model and an ordinary one-component Coulomb plasma, which is made clear after a sequence of steps. First, using partial integration and the boundary conditions, it follows that

$$\gamma\int d^2r(\vec{\nabla}h^*)^2=-\gamma\int d^2r\ h^*\nabla^2h^*. \quad (30)$$

Now, inserting Eq. (28) into this result gives

$$\gamma\int d^2r(\vec{\nabla}h^*)^2=-p\int d^2r\ h^*-ph_{\rm LK}\pi u^2, \quad (31)$$

where we have also used the pinning constraints (10). Finally, we insert Eq. (31) into Eq. (26) to obtain the energy of the membrane shape in mechanical equilibrium:

$$\begin{aligned}H^*_{\rm int}&=-\tfrac{1}{2}(\overline{h}-h_{\rm LK})\pi u^2+p(h_{\rm glyc}-h_{\rm LK})\pi u^2\\&=-\tfrac{1}{2}\gamma\int d^2r(\vec{\nabla}h^*)^2+p(h_{\rm glyc}-h_{\rm LK})\pi u^2, \quad (32)\end{aligned}$$

where we denoted the mean spacing by $\overline{h}$. Pursuing again the electrostatic analogy ($h\leftrightarrow\phi$, where ϕ is the electrostatic potential), we see that the first term of $H^*_{\rm int}$ indeed is like the electrostatic field energy $\int d^2r(\vec{\nabla}\phi)^2$, *except for a crucial difference in sign*. The ''Coulomb'' interaction between two like charges of our system (say, μ_1/γ and μ_2/γ) will thus be *attractive*.

We now derive the explicit dependence of $H_{\rm int}$ on $\{\vec{R}_i\}$. The first step is to solve Eq. (28) for the equilibrium membrane shape:

$$h^*(\vec{r})=-\frac{p}{4\gamma}r^2+\sum_{i=1}^{M}\left(\frac{\mu_i}{2\pi\gamma}\right)\ln\left(\frac{|\vec{r}-\vec{R}_i|}{a_0}\right)+h_0, \quad (33)$$

with a_0 a molecular cutoff length and h_0 a position-independent (but $\{\vec{R}_i\}$ dependent) constant of integration. The pinning constraints fix the set of $\{\mu_i\}$:

$$\begin{aligned}h_{\rm LK}=&-\frac{p}{4\gamma}\vec{R}_i^2+\sum_{j\neq i}^{M}\left(\frac{\mu_j}{2\pi\gamma}\right)\ln\left(\frac{|\vec{R}_i-\vec{R}_j|}{a_0}\right)+h_0\\&(i=1,\ldots,M). \quad (34)\end{aligned}$$

It is easy to show that for a homogeneous distribution of a large number charges, the Lagrange multipliers are all equal: $\mu_i=\mu$. For a thermodynamic state with only weak concentration fluctuations, the $\{\mu_i\}$ are approximately equal as well. We will assume $\mu_i=\mu$ for the remainder of the calculation and later test this assumption numerically. Note that under this condition, the constraints $h(\vec{R}_i)=h_{\rm LK}$ are obeyed *only on average*. We will discuss the validity of this approximation in Sec. VI.

Inserting Eqs. (33) and (28) into Eq. (32) gives us the final form for $H^*_{\rm int}$; we show only the explicit dependence on the LK locations:

$$\begin{aligned}H^*_{\rm int}(\vec{R}_1,\ldots,\vec{R}_M)=&-\frac{p\mu}{4\gamma}\sum_{i=1}^{M}(\vec{R}_i)^2\\&+\frac{\mu^2}{4\pi\gamma}\sum_{i\neq j}\ln\left(\frac{|\vec{R}_i-\vec{R}_j|}{a_0}\right)+\Delta, \quad (35)\end{aligned}$$

where Δ accounts for the $\vec{R}_i$-independent terms. The first term in this many-body Hamiltonian represents a parabolic single-particle potential that tends to push LK molecules to the edge. The second term is a logarithmic, *attractive* pair potential. Since the Coulomb interaction is indeed logarithmic in two dimensions, this confirms our earlier intuition. To make the electrostatic analogy more concrete, the dimensionless coupling constant of this many-body Hamiltonian $\mu^2/2\pi\gamma k_BT=p^2/2\pi\gamma k_BT[M]^2$ can be denoted q^2/k_BT.

In terms of $q=\mu/\sqrt{2\pi\gamma}$, we can write H^* as

$$H^*=-\frac{q^2}{2}M\sum_{i=1}^{M}\left(\frac{\vec{R}_i}{u}\right)^2+q^2\sum_{i>j}\ln\left(\frac{|\vec{R}_i-\vec{R}_j|}{u}\right)+\frac{3}{8}q^2M^2-\frac{q^2}{2}M\ln\left(\frac{u}{a_0}\right)+p(h_{\rm glyc}-h_{\rm LK})\pi u^2, \tag{36}$$

where we include the M- and u-dependent parts of Δ.

The number of adhesion molecules is not fixed. This means that the contribution to the free energy generated by $H^*_{\rm int}(\vec{R}_1,\ldots,\vec{R}_M)$, which we will call the correlation free energy, must be computed in the *grand canonical ensemble* with a chemical potential (controlled by E_B). In Secs. IV B and IV C we will first discuss the simpler case of correlations between LK molecules for a given M, i.e., for a fixed number of adhesion molecules.

B. Free energy

The M-particle free energy associated with H^* is given by

$$F=-k_BT\ln\left\{\frac{1}{a_0^{2M}M!}\prod_{i=1}^{M}\int_{|\vec{R}_i|<u,|\vec{R}_i-\vec{R}_j|>a_0}d^2\vec{R}_i e^{-\beta H^*}\right\} \tag{37}$$

up to a trivial constant. From Eq. (36) we see that the variables $\vec{R}_i$ enter in the dimensionless combination $\vec{z}_i=\vec{R}_i/u$. In terms of the $\vec{z}_i$ variables, the partition function takes the form

$$Z=\left(\frac{u}{a_0}\right)^{2M}\left(\frac{u}{a_0}\right)^{(\beta q^2/2)M}e^{-(3/8)\beta q^2M^2}\frac{1}{M!}\times\prod_{i=1}^{M}\int_{|\vec{z}_i|<1,|\vec{z}_i-\vec{z}_j|>a_0/u}d^2\vec{z}_i\,\exp\left(\frac{\beta q^2}{2}\sum_i|\vec{z}_i|^2-\beta q^2\sum_{i>j}\ln(|\vec{z}_i-\vec{z}_j|)\right). \tag{38}$$

Now take the thermodynamic limit $u\to\infty$, $M\to\infty$, with q finite. If the integral

$$\int_{|\vec{z}|<1}d^2z\;e^{-\beta q^2\ln|\vec{z}|} \tag{39}$$

exists, then we are allowed to set the (small) ratio a_0/u to zero in the second part of the partition function. The free energy in that case has the form

$$\frac{F}{M}=k_BT\ln([M]a_0^2)+\frac{q^2}{4}\ln([M]a_0^2)+\frac{q^2}{M}\Gamma(M,\beta q^2), \tag{40}$$

with $\Gamma(M,\beta q^2)$ a dimensionless function. If there exists a well-defined free energy per particle in the thermodynamic limit, then Γ must be proportional to M.

Suppose we keep the charge q fixed. All the dependence of F on the system size u then enters through the LK concentration $[M]$. We can then determine a ''fixed-q'' equation of state from Eq. (40). We define the 2D pressure $P_2=-\partial F/\partial(u^2\pi)|_q$. From Eq. (40) we find

$$P_2=[M]\left(k_BT+\frac{q^2}{4}\right). \tag{41}$$

This is the equation of state of an *ideal gas* with increased effective temperature $k_BT\Rightarrow k_BT+q^2/4$. The free energy has the general form of Eq. (40) only if the integral in Eq. (39) exists. This is true provided $\beta q^2<2$. For $\beta q^2\geqslant 2$, the integral diverges. We expect a phase transition at a temperature T_c with

$$k_BT_c=\frac{q^2}{2}. \tag{42}$$

For $q^2/k_BT\geqslant 2$, the free energy becomes highly sensitive to the value a_0 of the microscopic cutoff because of Eqs. (38) and (39), whereas for $q^2/k_BT<2$ it depends only logarithmically on a_0. In terms of the original variables, we can write the equation of state for $\beta q^2<2$ as

$$P_{2D}=k_BT[M]+\frac{p^2}{8\pi\gamma[M]}, \tag{43}$$

while the phase transition should occur at

$$k_BT_c=\frac{p^2}{8\pi\gamma[M]^2}. \tag{44}$$

V. DEBYE-HÜCKEL THEORY

In the Bell model, it is assumed that the LK molecules are uniformly distributed over the adhesion disk. In this section, we will borrow a classical method of plasma physics, Debye-Hückel (DH) theory [26], to compute the correlation free energy of the uniform state and simultaneously test the stability of this state. We will assume that the dimensionless coupling constant q^2/k_BT is small, so we are really doing a perturbation expansion around the ideal solution theory of Sec. III. Following DH theory [26], we start by placing an LK molecule (say $i=1$) at the origin and keep it fixed. We now want to calculate the thermally averaged height profile $\langle h(\vec{r})\rangle_1$ surrounding the fixed charge. The function $\langle h(\vec{r})\rangle_1$ will be assumed to obey the condition

$$\lim_{|\vec{r}|\to a_0}\langle h(\vec{r})\rangle_1=h_{\rm LK}+\frac{\mu}{2\pi\gamma}\ln\left(\frac{r}{a_0}\right)+\cdots. \tag{45}$$

We also will assume that, far from the origin, the spacing profile is flat and equal to the average spacing so

$$\lim_{|\vec{r}|\to\infty}\langle h(\vec{r})\rangle_1=\langle\overline{h}\rangle, \tag{46}$$

with $\langle\overline{h}\rangle$ the thermal average of the mean spacing $\overline{h}$. The first condition is the pinning constraint applied to the edge of the LK complex plus the requirement that for $r\simeq a_0$ the height profile must be that of a single LK molecule. The second reflects the requirement that the effects of a molecule at the origin will be screened at large distances. From Eq. (28) we find that

$$\gamma\nabla^2\langle h(\vec{r})\rangle_1=-p+\rho(\vec{r})+\mu\delta(\vec{r}), \tag{47}$$

with

$$\rho(\vec{r}) \equiv \mu \left\langle \sum_{i=2}^{M} \delta(\vec{r} - \vec{R}_i) \right\rangle \tag{48}$$

proportional to the thermally averaged density of LK molecules: the ''charge density'' of the screening cloud in the electrostatics picture. Using Eq. (29), the ''charge neutrality'' condition, we find a normalization condition for $\rho(\vec{r})$,

$$\frac{\int d^2r\ \rho(\vec{r})}{\pi u^2} = p\left(1 - \frac{1}{M}\right). \tag{49}$$

Now we assume that the thermally averaged LK density follows the Boltzmann distribution

$$\rho(\vec{r}) = p e^{-\Delta U(\vec{r})/k_B T}, \tag{50}$$

where $\Delta U(\vec{r})$ is the thermally averaged potential energy cost of moving an LK molecule from infinity to $\vec{r}$. On the basis of our electrostatic analogy ($h \leftrightarrow \phi$ and $\mu \leftrightarrow q$), we would expect

$$\Delta U(\vec{r}) = (\langle h(\vec{r})\rangle_1 - \langle \overline{h} \rangle)\mu. \tag{51}$$

In the Appendix we show that this indeed is the right choice. The average density profile is then taken to be

$$\rho(\vec{r}) = p\ \exp\left\{ -\frac{\mu}{k_B T} [\langle h(\vec{r})\rangle_1 - \langle \overline{h} \rangle] \right\}. \tag{52}$$

If we linearize the exponential in the expression for $\rho(\vec{r})$ in the limit of high temperature and insert this into Eq. (47), we obtain the inhomogeneous differential equation

$$\nabla^2 \langle h \rangle_1 = -\left(\frac{p\mu}{\gamma k_B T}\right)(\langle h \rangle_1 - \langle \overline{h} \rangle). \tag{53}$$

The general radially symmetric solution to Eq. (53) is

$$\langle h \rangle_1 = A J_0(\kappa r) + B N_0(\kappa r) + \langle \overline{h} \rangle, \tag{54}$$

where

$$\kappa = p([M]\gamma k_B T)^{-1/2} \tag{55}$$

is an inverse length and J_0 and N_0 are Bessel functions with A and B integration constants. The quantity κ is formally analogous to the inverse Debye screening length. This is better seen in the ''electrostatic'' language, where Eq. (55) reduces to

$$\kappa^2 = \frac{2\pi[M]q^2}{k_B T}, \tag{56}$$

which is of the form of the usual definition of the Debye parameter. Note that for coupling constants $q^2/k_B T$ of order one, κ^{-1} is of order the LK-LK spacing. For the *repulsive* Coulomb plasma, however, correlations decay exponentially fast for distances large compared to κ^{-1}, whereas in our case they decay only as an oscillatory power law proportional to $\cos(\kappa r + \phi)/r^{1/2}$.

To determine the integration constants A and B, we first note that

$$\lim_{x \to 0} N_0(x) = \frac{2}{\pi}(\ln x + \gamma_E - \ln 2), \tag{57}$$

with $\gamma_E = 0.577\ldots$ Euler's constant. To obey Eq. (45) in the limit $\kappa r \ll 1$, we thus must demand that in Eq. (54)

$$B = \frac{\mu}{4\gamma}. \tag{58}$$

Next we must demand that $\langle h(\vec{r})\rangle_1$ is flat at $r = u$. This is the case if

$$A J_1(\kappa u) + B N_1(\kappa u) = 0. \tag{59}$$

The complete solution for $\langle h(\vec{r})\rangle_1$ is then

$$\langle h(\vec{r})\rangle_1 = \langle \overline{h} \rangle + \frac{\mu}{4\gamma}\left\{ N_0(\kappa r) - \left(\frac{N_1(\kappa u)}{J_1(\kappa u)}\right) J_0(\kappa r) \right\}. \tag{60}$$

The second term of Eq. (60) is the correction to the mean spacing $\langle \overline{h} \rangle$ introduced by the fixed charge at the origin. We will examine this correction term, starting from the high-temperature limit where $\kappa \to 0$ [see Eq. (56)]. If $\kappa u \ll 1$, we can set $J_0(\kappa r) \approx 1$ since $r \leqslant u$, while for $N_0(\kappa r)$ we can use Eq. (57):

$$\langle h(\vec{r})\rangle_1 \cong \langle \overline{h} \rangle + \frac{\mu}{2\pi\gamma}[\ln(\kappa r) + \gamma_E - \ln 2] + \frac{\mu}{\pi\gamma(\kappa r)^2}. \tag{61}$$

The correction term has a logarithmic profile similar to that of a single, isolated LK molecule. Note though that for $\kappa u \to 0$ the correction term diverges so the applicability of perturbation theory is suspect. As we increase κu, matters get even worse. When κu approaches the first zero $x_1 \cong 3.8$ of the J_1 Bessel function, the correction term in Eq. (60) mathematically diverges. We must conclude that for $\kappa u \geqslant 3.8$, the uniform state is unstable. This is a very severe constraint. Using Eq. (56) we can write the unstable range as

$$\frac{q^2}{k_B T} \geqslant \frac{7.2}{M}. \tag{62}$$

Apparently, in the thermodynamic limit $M \to \infty$ the uniform state is unstable *for any fixed value* of the coupling constant $q^2/k_B T$. We will investigate in Sec. VI what happens for finite values of $q^2/k_B T$. It is, however, still useful to compute the free energy using the DH method. This is done by demanding that $\langle h(|\vec{r}| = a_0)\rangle_1 = h_{\mathrm{LK}}$ in Eq. (60). This requirement fixes the mean spacing $\langle \overline{h} \rangle$:

$$\langle \overline{h} \rangle \cong h_{\mathrm{LK}} - \frac{\mu}{2\pi\gamma}\{\ln(\kappa a_0) + \gamma_E - \ln 2\} + \frac{\mu}{4\gamma}\frac{N_1(\kappa u)}{J_1(\kappa u)}. \tag{63}$$

Inserting Eq. (63) into Eq. (32) gives the internal energy $E_{\mathrm{int}} = \langle H^*_{\mathrm{int}} \rangle$:

$$\frac{E_{\rm int}}{\pi u^2} = p(h_{\rm glyc} - h_{\rm LK}) + \frac{\mu p}{4\pi\gamma}\{\ln(\kappa a_0) + \gamma_E - \ln 2\} - \frac{\mu p}{8\gamma}\left(\frac{N_1(\kappa u)}{J_1(\kappa u)}\right). \quad (64)$$

The second and third terms represent the contribution to $E_{\rm int}$ from correlations. Note the divergence when $\kappa u \cong 3.8$. In electrostatic language, we can write Eq. (64) as an energy per particle:

$$\frac{E_{\rm int}}{M} = \frac{q^2}{4}\ln([M]a_0^2) + \frac{q^2}{2}\left\{\frac{1}{2}\ln\left(\frac{2\pi q^2}{k_B T}\right) + \gamma_E - \ln 2\right\} - \frac{\pi}{2}q^2\frac{N_1\left(\sqrt{\frac{2Mq^2}{k_B T}}\right)}{J_1\left(\sqrt{\frac{2Mq^2}{k_B T}}\right)}, \quad (65)$$

dropping the trivial term in Eq. (64). Equation (65) has exactly the right general form required by Eq. (40). Because the last term depends explicitly on M, there is in general no well-defined energy per particle in the thermodynamic limit, another sign of the instability of the uniform state. However, in the high-temperature limit, the last term in Eq. (65) is inversely proportional to M and it only contributes a *constant* term, of order $k_B T$, to $E_{\rm int}$, which can be dropped. In the $\kappa u \to 0$ limit we then find a well-defined correlation free energy per unit area

$$\frac{F_{\rm int}}{\pi u^2} = \frac{p^2}{4\pi\gamma[M]}\left\{\frac{1}{2}\ln\left(\frac{p^2 a_0^2}{[M]\gamma k_B T}\right) + \gamma_E - \ln 2 - \frac{1}{2}\right\}. \quad (66)$$

The complete DH free energy per unit area $f([M])$ for fixed M is then

$$f([M]) = k_B T[M]\ln([M]a) - \frac{p^2}{8\pi\gamma[M]}\ln\left(\frac{\gamma k_B T}{\Gamma p^2 a_0^2}[M]\right). \quad (67)$$

We will use Eq. (66) as the correlation free energy to study the weak-coupling limit.

VI. NUMERICAL SIMULATIONS

We have preformed Monte Carlo numerical simulations on the many-body Hamiltonian $H^*_{\rm int}(\vec{R}_1,\ldots,\vec{R}_M)$ of Eq. (35). The aim of the numerical work was threefold: (i) to examine the regime of finite $q^2/k_B T$ values that was not accessible by the DH method, (ii) to verify the predictions of the DH method for the weak-coupling regime, and (iii) to examine the validity of the assumption that we could set the Lagrange multipliers μ_i to be equal to μ.

Our first simulations were done with the μ_i values set to μ and the number of LK molecules M fixed at $M = 25$, in a disk of fixed radius (canonical ensemble). We used the standard Metropolis algorithm with small random updates (microsteps) in the successive positions of the particles. Typical equilibrium configurations are shown in Figs. 4(a)–4(c) in which the system had been allowed to equilibrate for 5000 sweeps (125 000 updates). The particle positions in Figs. 4(a)–4(c) correspond to dimensionless coupling constants $e^2/k_B T$ (or $\mu^2/2\pi k_B T$) equal to 0 [Fig. 4(a)], 0.11 [Fig. 4(b)], and 0.15 [Fig. 4(c)].

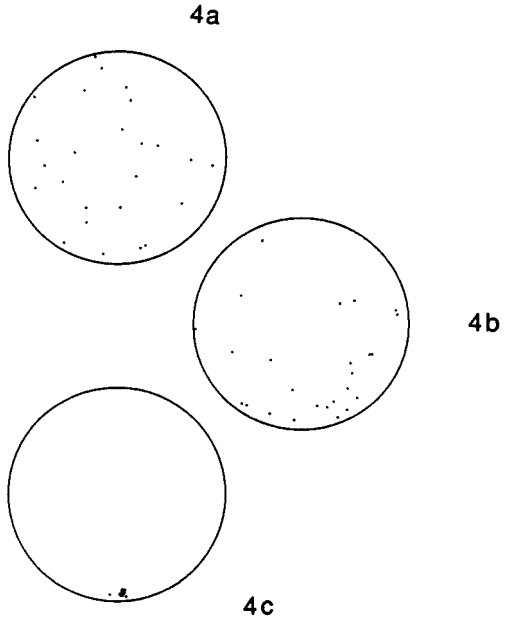

FIG. 4. Snapshots of a 25-particle Monte Carlo simulation. The dimensionless coupling constant $q^2/k_B T$ equals (a) 0.0, (b) 0.11, and (c) 0.15.

In Fig. 4(a) the particles assume random positions corresponding to a dilute two-dimensional gas. In Fig. 4(b) we see the effect of increased attraction: the LK molecules have a tendency to cluster and some appear bound in pairs. Note that the density of LK molecules is higher at the edge due to the inverse parabolic single-particle potential of Eq. (35). However, if we watch a particular molecule, it will wander over the whole disk given sufficient time. Finally, in Fig. 4(c) a small increase in the coupling constant has led to total collapse: All particles are collected into a single dense patch, the stress-focused state. The cluster appears to be nearly immobile and is located at the sample edge for reasons discussed above. We infer that there is a critical value for the coupling constant, between 0.11 and 0.15, marking a phase transition between an extended and a localized state of the many-body system.

These results lead us to the following conclusions. For small but finite values of $q^2/k_B T$, the LK molecules explore the adhesion disk, but the average concentration has a *nonuniform* profile $[M](\vec{r})$, which is small at the center of the adhesion disk and large at the edge. This violates the basic assumption of the perturbative DH theory. The collapse of the adhesion molecules around $q^2/k_B T \cong 0.15$ appears to be consistent with the theoretical prediction that for $q^2/k_B T \geqslant 2$, the free energy should be sensitively dependent on the short-distance cutoff a_0 for the replusive potential. We do not know, however, why the collapse happens already around 0.15 rather than 2.

Next we allowed the number of adhesion molecules M to vary. A given configuration of M particles on a disk of radius u was assigned the probability

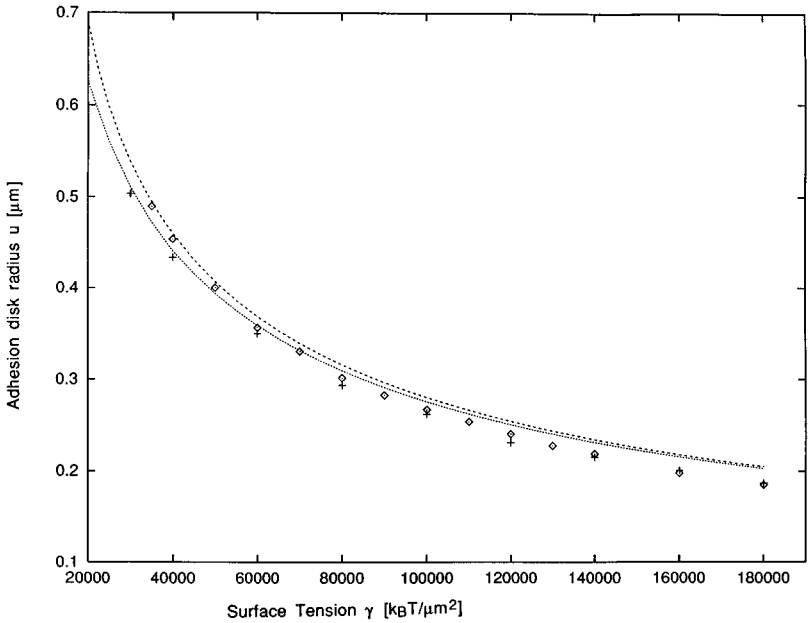

FIG. 5. Result of Monte Carlo simulations with variable particle number (weak coupling). The average adhesion disk radius u is shown as a function of the tension. The lower dotted curve is the prediction of ideal solution theory (Bell model). The upper dashed curve includes corrections from DH theory. The data marked + correspond to $q^2/k_BT=0$. The deviations from ideal solution theory for large γ are due to finite-size effects. The data marked $\diamond$ correspond to simulations of the interacting case with $p=6\times10^3 k_BT/\mu\mathrm{m}^3$.

$$P[\{\vec{R}_j\},M,u]=Z^{-1}\left[\frac{4\pi R^2/a'}{(N-M)!}\right]^2\left[\frac{\pi u^2/a}{M!}\right]\exp\{-(1/k_BT)\times[\Delta H_{\mathrm{el}}+H_{\mathrm{glyc}}+H_{\mathrm{LK}}]\}. \tag{68}$$

We then varied not only the particle positions, but in this case also the disk radius u and the particle number M. Note that we cannot specify the coupling constant, which depends on $[M]$. Since the LK concentration is self-adjusting, the system ''chooses'' its own coupling constant.

The results of our simulation are shown in Fig. 5, where we plot the equilibrium disk radius u^* (in micrometers) as a function of the tension γ (in units of $k_BT/\mu\mathrm{m}^2$) for fixed vesicle radius $R=10$ μm. The lower of the two curves is the u^* prediction of Young's law $u^*=R(2G/\gamma)^{1/2}$ with $G=G_{\mathrm{IS}}$ [see Eqs. (8) and (24)], that is, neglecting the indirect interactions. The data marked by pluses are the result of the simulation, also neglecting interaction. For smaller γ, the agreement between theory and simulation is good, while for large γ theory underestimates u^* systematically. This is due to the fact that for large γ both the disk radius and the number of LK molecules become small, so finite-size corrections become important. The average number of LK molecules for our largest γ ($1.8\times10^5 k_BT/\mu\mathrm{m}^2$) was approximately 12.36, while for our smallest γ ($3.5\times10^4 k_BT/\mu\mathrm{m}^2$) it was 81.8.

Next we turned to the LK coupling. The upper dashed curve is the prediction of DH theory by using Eq. (66). The coupling leads to a modest increase in contact area. The increase agrees with our data (marked by diamonds), but only for the smaller tensions. At higher tensions, finite-size corrections exceed the DH correction (which decreases with increasing tension). We chose a fixed value of p ($6\times10^3 k_BT/\mu\mathrm{m}^3$) such that the coupling constant was always small. The largest coupling constant, corresponding to the smallest γ data point, was only $q^2/k_BT=1.46\times10^{-2}$. The grand canonical simulations consisted of up to 5×10^7 updates (microsteps) with measured autocorrelation times of (5×10^3)–(5×10^4) updates.

Finally, we examined the validity of the assumption constant μ_i ($\mu_i=\mu$). We performed the check with M fixed (at $M=20,40$) and with M self-adjusting, although u was fixed in both cases. We also allowed a range of coupling constants q^2/k_BT from 10^{-2} to 4×10^{-1}. At every Monte Carlo microstep we solved the set of M linear equations [Eq. (10)] for the $\{\mu_i\}$. Analyzing the distribution of fluctuations, we found that the standard deviation was substantial, about 25% of the average value, for the weak-coupling regime. The important thermodynamic quantity $[M]$, however, showed only small deviations from the mean-field (fixed μ) prediction. These results indicate that the fixed μ theory could be questioned on this basis, in particular near the collapse transition where substantial concentration fluctuations are observed [see Fig. 4(b)], and more numerical work is necessary.

VII. PHASE DIAGRAM AND CONCLUSION

We will now use the results of the preceding section to construct a phase diagram for adhesion that includes the effects of correlations. This phase diagram will have the tension γ of the vesicles as the horizontal axis and the disjoining pressure p as the vertical axis.

The procedure we will follow is similar to the one described in Sec. II. The free energy is

$$\Delta F(u)=-G\pi u^2+2\pi\tau u+\pi\gamma\frac{u^4}{R^2}, \tag{69}$$

where

$$G = G_{\rm IS} - \frac{F_{\rm int}}{\pi u^2}, \tag{70}$$

with $F_{\rm int}$ the LK correlation free energy and $G_{\rm IS}$ the ideal-solution adhesion energy. We must minimize $\Delta F(u)$ with respect to u. A finite u minimum is associated with collective adhesion and a $u=0$ minimum with separation or microadhesion.

A. Weak-binding regime

We will first establish the phase diagram for the case that the number of LK molecules M is small compared to the available number N. The unbound L and K molecules act like a reservoir in chemical equilibrium with the LK molecules (see Sec. III). Under these conditions, we can use Eq. (24) for $G_{\rm IS}$, with M given by Eq. (22).

We will start in the regime of high tension γ where the dimensionless coupling constant is small. In that regime, we use the DH correlation free energy (66) in Eq. (70):

$$\begin{aligned} -G([M]) \simeq & k_B T [M] \ln\left([M] \frac{a}{e} \right) \\ & + \left\{ k_B T \ln\left(\frac{1}{[N]^2 a'^2} \right) - E_B \right\} [M] \\ & - \frac{p^2}{8\pi\gamma[M]} \ln\left(\frac{\gamma k_B T}{\Gamma p^2 a_0^2} [M] \right) + p\Delta h, \end{aligned} \tag{71}$$

where $\Delta h = h_{\rm glyc} - h_{\rm LK}$. First minimizing ΔF with respect to $[M]$ gives a LK concentration

$$[M] \cong [M_{\rm IS}] - \frac{p^2}{16\pi k_B T [M_{\rm IS}]} \ln\left[\frac{[M_{\rm IS}]\gamma k_B T}{e\Gamma p^2 a_0^2} \right], \tag{72}$$

with $[M_{\rm IS}]$ the LK concentration in the absence of correlations ($[M_{\rm IS}] = [N]^2 (a'^2/a)^2 e^{E_B/k_B T}$). Inserting Eq. (72) back into Eq. (71) gives a threshold $p_T(\gamma)$ for separation where $G=0$ (see Sec. II):

$$p_T(\gamma) \cong p_T^{(0)} \left[1 + \frac{k_B T}{16\pi\gamma\Delta h^2} \ln\left(\frac{[M_{\rm IS}]\gamma k_B T}{\Gamma (p_T^0)^2 a_0^2} \right) \right], \tag{73}$$

with $p_T^{(0)}$ the separation threshold in the absence of correlations given by Eq. (24). Correlations thus *increase* the adhesive strength since the argument of the logarithm is of order $1/[M]_{\rm IS} a_0^2$, which is large compared to one. The enhancement factor of the threshold pressure is of order $k_B T/\gamma\Delta h^2$, which grows with decreasing γ as $1/\gamma$.

As we reduce γ, the coupling constant $q^2/k_B T$ starts to increase. The adhesion disk should collapse when $q^2/k_B T = 2$ according to Eq. (42), or even earlier according to the numerical simulations of Sec. VI. Using $q^2/k_B T = 2$, the transition should occur when $p = p(\gamma)$, with

$$p(\gamma) = [M]\sqrt{8\pi\gamma k_B T}. \tag{74}$$

To estimate $p(\gamma)$, we use $[M] = [M]_{\rm IS}$

$$p(\gamma) \approx [N] \left(\frac{a'^2}{a} \right)^2 e^{E_B/k_B T} \sqrt{8\pi\gamma k_B T}, \tag{75}$$

in which case $p(\gamma) \propto \gamma^{1/2}$.

Although the DH adhesion energy is not to be trusted for finite values of $q^2/k_B T$, it is interesting to note that $\partial^2/\partial[M]^2$ acting on $-G([M])$ is positive for $q^2/k_B T$ small, while around $q^2/k_B T$ of order one, $-(\partial^2/\partial[M]^2)G([M])$ becomes negative. This indicates that the collapse transition may be signaled by spinodal decomposition.

In the collapsed state, the LK molecules are collected in a single small patch. The collapse will suppress any billowing out between LK molecules, so $h(\vec{r}) \simeq h_{\rm LK}$ in the patch, while the vesicles are spherical. The adhesion energy can then be only weakly dependent on γ, so the fracture pressure $p_T(\gamma)$ of the collapsed state is expected to be *independent* of γ. The fracture pressure of the collapsed state should be (crudely) given by Eq. (73) with γ replaced through γ_0 defined by $p_T^{(0)} \approx [M]_{\rm IS}\sqrt{8\pi\gamma_0 k_B T}$. The resulting phase diagram was shown already in Fig. 1. The saturation tension γ_0 is of order $k_B T/\Delta h^2$.

B. Strong-binding regime

As we increase the LK binding energy, we absorb more and more of the adhesion molecules into the adhesion disks. Eventually, we exhaust the supply when M grows to be of order N. The condition for this to happen is that $[M]_{\rm IS}$ given by Eq. (22) exceeds $N/\pi u^2$, which is the case if

$$\frac{E_B}{k_B T} \geqslant \ln\left(\frac{4aR^2}{[N]a'^2 u^2} \right). \tag{76}$$

The adhesion disk is then in a canonical ensemble with $M \approx N$. The discussion of the phase diagram proceeds along the same lines and the results are qualitatively similar. There are, however, a number of quantitative differences: The large γ threshold pressure is $p_T^{(0)} \approx E_B/\Delta h a_0^2$, the enhancement of the threshold pressure in the collapsed regime $q^2/k_B T \geqslant 1$ is of order $E_B/\gamma\Delta h^2$, and the bounding line between weak and strong coupling is $p(\gamma) \approx \gamma (N/2\pi R^2)^{1/2}$ for small γ is proportional to γ (rather than to $\gamma^{1/2}$).

In summary, our results demonstrate that the ideal-solution assumption for the LK molecules, as well as the assumption of homogeneity for the adhesion disk, is fundamentally incorrect. No matter how small the coupling constant $q^2/k_B T$, i.e., no matter how large the membrane tension, the adhesion disk is necessarily inhomogeneous with most adhesion molecules clustered around the rim. We believe that this organization of the adhesion disk is a generic phenomenon for the competitive adhesion description embodied in the Bell model. For lower tensions, the deviations from the noninteracting model are severe. If the tension $\gamma \leqslant k_B T/\Delta h^2$, then loss of adhesion proceeds via a collapsed state. The collapsed state has an adhesive strength that is enhanced by a factor of $k_B T/\gamma\Delta h^2$ for weak binding and $E_B/\gamma\Delta h^2$ for strong binding. The collapsed state can be viewed as an extreme example of stress focusing.

To apply our results to actual bioadhesion, we need to assign values to γ, E_B, p, R, and $[N]$. Starting with the distinction between weak and strong binding, measured val-

ues of E_B/k_BT for adhesion molecules range from 5 (selectin-carbohydrate binding) to 35 (biotin-streptavidin) as discussed in Sec. I. Typical area densities of adhesion molecules are about 1/200 Å^2 so on a spherical vesicle of radius $R=10\ \mu$m, there would be of order $N=10^4$ adhesion molecules. The length of an adhesion molecule is in the range 100–200 Å, so the effective reactive area a'^2/a should be of order 100 Å^2. For an adhesion disk of radius $u\sim 1\ \mu$m, the weak-binding range is then $E_B/k_BT\leqslant 10$ according to Eq. (76). Both weak and strong binding are thus realistic possibilities for vesicle unbinding.

The next question is whether the predicted stress-focusing transition is in a realistic range of parameters. From the phase diagram Fig. 1, one sees that for tensions $\gamma \leqslant k_BT/\Delta h^2$, the collapsed state is a necessary intermediate in the unbinding scenario of vesicles. White blood cell tensions have been measured and were found to be in the range of 10^{-2} erg/cm^2. Red blood cell tensions are so low that they could not be measured. If the glycocalix compression is less than 100 Å, which seems very reasonable since that is the size of the adhesion molecules, then $\gamma<k_BT/\Delta h^2$ and the collapsed state should indeed be encountered in Fig. 1 on increasing the disjoining pressure.

One particularly interesting experiment on vesicle adhesion was performed by Chiruvolu *et al.* [27] using biotin-streptavidin bonding on 500-Å vesicles with about 80 links between the vesicles. Using $a=a'=20\ \text{Å}^2$ and $E_B/k_BT \simeq 30$, we should be deep in the strong-binding regime. The vesicles in the experiment were nominally tensionless so the adhesion disk should be collapsed into a small patch. Optical studies of biotin-streptavidin vesicle aggregation are in good agreement with this prediction. The disjoining pressure p is not due to a glycocalix. However, thermal fluctuations produce a Helfrich entropic repulsion with a similar effect. It would be interesting to add PEG lipids to these vesicles, which could act as an artificial glycocalix.

It is also interesting to speculate on possible biological relevance of stress focusing. According to our results, adhesion molecules are likely to aggregate into a single patch. For killer T cells, adhesion molecules of the T cell surface bond to partner molecules in the target cells called the major histocompatibility complex. Once the bond has been established, the adhesion molecules trigger the release of lysis agents that destroy the target cell membrane. In the collapsed state, the release of lysis agents on a focused section of the target membrane would be considerably more effective. In addition, the stress-enhancement factor $E_B/\gamma\Delta h^2$ for strong coupling is order 10^3 for $\gamma\sim 10^{-2}$ erg/cm^2, $\Delta h\sim 10$ Å, and $E_B/k_BT\sim 20$. The stress-focused state is thus expected to be far stronger than the homogeneous adhesion disk envisaged by Bell and co-workers [10].

Adhesion in biological tissue in general does not involve just two cells but rather the coordinated organization of large numbers of cells and the use of a study of adhesion between pairs of cells appears to be limited to *in vitro* studies. Knowledge concerning adhesion energies between pairs of cells can, however, give important insights into the organization of cells. In the ''thermodynamic'' model of cell sorting during embryogenesis of Steinberg [28] for instance, tissue organization of neural retina cells was found to be based on the hierarchy of cell adhesion energies of the various cells. Differences in cellular adhesion energies are attributed to variations in the concentration of the adhesion molecules on the cell surface or in the type of adhesion molecules [29]. In the present study we have found that the adhesion energy of a cell also may be modulated by varying the glycocalix repulsion or externally applied stresses. Tissue organization in stressed tissue thus could be different from that of unstressed tissue.

A second area of possible biological relevance concerns the early stages of formation of clusters of adhesion molecules (such as cadherins) in epithelial cells. Under ordinary ''static'' conditions these adhesion molecules are usually connected to the cytoskeleton. However, during the early stages of the formation of the adhesive link between two cells, the adhesion molecules may cluster in groups by the membrane-mediated attraction mechanism discussed in this paper. This clustering could then be followed by the connection to the cytoskeleton. It should be noted that in general there are several junctions along the adhesion area between two epithelial cells. This could be a natural consequence of the decompositional kinetics of the collapse transition, with disconnected clusters forming in separate area's. The authors however, are not aware of studies of early stages of adhesive links in epithelial cells.

A general problem for the verification of the predictions of this paper for living cells is presented by the dynamical nature of adhesive links. After molecular recognition between an adhesion molecule and its ligand, formation of cytoskeletal links can, as mentioned, alter the surface energies. Also, at the molecular level, studies of adhesion molecules under stress demonstrate that they respond in a time-dependent fashion: The fracture of the link between an adhesion molecule and its ligand also is known to depend on the observation period [30].

ACKNOWLEDGMENTS

D.Z. would like to thank Benjamin P. Lee and Xiao-jun Li for helpful discussions. He is also grateful for the advice and support (under NSF Grant No. CHE 93-11729) of Professor Michael E. Fisher. R.B. would like to acknowledge NSF support under Grant No. DMR 9708646 and the hospitality of the ITP. He would like to thank J. Israelachvili, E. Sackmann, and C. Safinya for helpful discussions and J. Wilhelm (Technische Universität Münich) for discussing the derivation of Eq. (32).

APPENDIX: MEAN POTENTIAL

To find the potential energy ΔU of a charge brought in from infinity to $\vec{R}$, with a fixed charge at the origin, we fix two charges in place ($i=1$ at $\vec{r}=0$ and $i=2$ at $\vec{r}=\vec{R}$) and allow the remaining charges to reach thermal equilibrium. In the limit $\vec{R}\to 0$, the two charges interact via their ''bare'' logarithmic attractive potential [see Eq. (35)] so

$$\Delta U(\vec{R}) \approx \frac{\mu^2}{2\pi\gamma} \ln\left(\frac{|\vec{R}|}{\xi}\right) + \text{const} \quad \text{for } |\vec{R}|\to 0. \quad \text{(A1)}$$

Since the averaged height profile $\langle h(\vec{r})\rangle_1$ around a single charge obeys, for small r,

$$\langle h(\vec{r})\rangle_1 \approx \frac{\mu}{2\pi\gamma}\ln(r/\xi)+\text{const}, \tag{A2}$$

we can combine Eqs. (A1) and (A2) as

$$\Delta U(\vec{R}) \approx \mu\langle h(\vec{R})\rangle_1 + \text{const} \quad \text{for } |\vec{R}|\to 0. \tag{A3}$$

It should be noted though that our mean-field assumption $\mu_i=\mu$ is questionable when two charges approach closely. To find the large-$|\vec{R}|$ limit of $\delta U(\vec{R})$, let $\langle h(\vec{j})\rangle_2$ be the spacing profile around the two charges. In the limit $\vec{R}\to\infty$,

$$\langle h(\vec{r})\rangle_2 \approx \langle h(\vec{r})\rangle_1 + \langle h(\vec{r}-\vec{R})\rangle_1 - \langle h\rangle \tag{A4}$$

since the ''charge clouds'' surrounding the two fixed charges do not mutually deform each other. Inserting Eq. (A4) into Eq. (32) gives the internal energy $U_2(\vec{R})$:

$$U_2(\vec{R}) \simeq -\frac{\gamma}{2}\int d^2r[\vec{\nabla}\langle h(\vec{r})\rangle_2]^2 + \text{const} \tag{A5}$$

$$\simeq 2U_1 + \frac{\gamma}{2}\int d^2r\{\langle h(\vec{r})\rangle_1\nabla^2\langle h(\vec{r}-\vec{R})\rangle_1 + \langle h(\vec{r}-\vec{R})\rangle_1\nabla^2\langle h(\vec{r})\rangle_1\} + \text{const},$$

with u_1 the energy cost of a single charge.

We now note that $\nabla^2\langle h(\vec{r})\rangle_1$ is strongly peaked at the position of the charge:

$$\nabla^2\langle h(\vec{r})\rangle_1 = \frac{\mu}{\gamma}\,\delta(\vec{r}) + (\text{regular terms}). \tag{A6}$$

Using Eq. (A6) in Eq. (A5) gives, for $R\to\infty$,

$$U_2(\vec{R}) \approx 2u_1 + \mu[\langle h(\vec{R})\rangle_1 - \overline{\langle h\rangle}]. \tag{A7}$$

The constant is determined by the condition that $U_2(\infty)=2U_1$. Hence we conclude that

$$\Delta U(\vec{R}) \approx \mu[\langle h(\vec{R})\rangle_1 - \overline{\langle h\rangle}] \quad \text{for } R\to\infty, \tag{A8}$$

which is consistent with Eq. (A3). In the body of the paper, we therefore use the identification

$$\Delta U(\vec{R}) \approx \mu[\langle h(\vec{R})\rangle - \overline{\langle h\rangle}] \tag{A9}$$

for all $\vec{R}$.

[1] L. E. Hood, I. L. Weissman, W. B. Wood, and J. H. Wilson, *Immunology*, 2nd ed. (Benjamin, Menlo Park, CA, 1984).

[2] G. Edelman, *Topobiology: An Introduction to Molecular Embryology* (Harper Collins, New York, 1988).

[3] See, for instance, N. Wang, J. P. Butler, and D. E. Ingbar, Science **260**, 1124 (1993).

[4] V. T. Moy, E.-L. Florin, and H. E. Gaub, Science **266**, 257 (1994).

[5] D. E. Leckband, J. N. Israelachvili, F.-J. Schmitt, and W. Knoll, Science **255**, 1419 (1992).

[6] E. A. Evans, K. Ritchie, and R. Merliel, Biophys. J. **68**, 2580 (1995); L. A. Sung and E. A. Kabat, Biorheology **31**, 353 (1994).

[7] E. A. Evans (private communication).

[8] W. I. Weis (private communication).

[9] See, for instance, J. Monod, *Le Hasard et la Nécesité* (Editions du Seuil, Paris, 1970), Chaps. 3 and 4.

[10] G. I. Bell, Science **200**, 618 (1978); G. I. Bell, M. Dembo, and P. Bongrand, Biophys. J. **45**, 1051 (1984).

[11] J. Israelachvili, *Intermolecular and Surface Forces: With Applications to Colloidal and Biological Systems* (Academic, London, 1985).

[12] R. Bruinsma, in *Physics of Biomaterials*, *NATO Advanced Study Institute Winter School* (Plenum, New York, 1995).

[13] A. Adamson, *Physical Chemistry of Surfaces* (Wiley, New York, 1982), Chap. II.

[14] E. A. Evans, Biophys. J. **48**, 185 (1985); **48**, 175 (1985).

[15] U. Seifert and R. Lipowsky, Phys. Rev. A **42**, 4768 (1990).

[16] J. Radler, T. Feder, H. Strey, and E. Sackmann, Phys. Rev. E **51**, 4526 (1995).

[17] D. A. Hammer and D. Lauffenburger, Biophys. J. **52**, 475 (1987); C. Zhu, J. Theor. Biol. **150**, 27 (1991).

[18] A. Tozeren, K.-L. Sung, and S. Chien, Biophys. J. **55**, 479 (1989).

[19] V. L. Chen, C. Helm, and J. Israelachevilli, J. Phys. Chem. **95**, 10726 (1991).

[20] A. Baljon and M. Robbins, Science **271**, 482 (1996).

[21] J. Braun, J. Abney, and J. Owicki, Nature (London) **310**, 316 (1984); J. Abney, J. Braun, and J. Owicki, Biophys. J. **52**, 441 (1987).

[22] R. Bruinsma, M. Goulian, and P. Pincus, Biophys. J. **67**, 746 (1994).

[23] D. Zuckerman and R. Bruinsma, Phys. Rev. Lett. **74**, 3900 (1995). Our previous study focused on a special fixed–average-membrane-spacing ensemble in which case we find *repulsive* indirect LK interactions.

[24] For a discussion of mobility of adhesion molecules see E. J. Luna and A. L. Hitt, Science **258**, 955 (1992); L. A. Lasky, M. S. Singer, D. Dowbenko, Y. Imai, W. Hensel, C. Fennie, S. Watson, and S. Rosen, *Cold Spring Harbor Symposia on Quantitative Biology* (Cold Spring Harbor Laboratory, Cold Spring Harbor, 1992), Vol. LVII; M. McCloskey and M. M. Poo, J. Cell. Biol. **102**, 2185 (1986).

[25] W. Helfrich, Z. Naturforsch. A **33**, 305 (1978).

[26] See, for instance, D. A. McQuarrie, *Statistical Mechanics* (Harper Collins, New York, 1976), Chap. 15.

[27] S. Chirovolu *et al.*, Science **264**, 1753 (1994).

[28] M. S. Steinberg, J. Exp. Zool. **173**, 395 (1970); K. Crawford and D. L. Slocum, Development **102**, 687 (1988).

[29] For a review see S. F. Gilbert, *Developmental Biology* (Sinauer, Sunderland, MA, 1994), Chap. 3.

[30] E. Evans and K. Ritchie, Biophys J. (to be published).